

Seismic evidence of a complex multi-lens melt reservoir beneath the 9° N Overlapping Spreading Center at the East Pacific Rise

A. F. Arnulf, S. C. Singh, J. W. Pye

▶ **To cite this version:**

A. F. Arnulf, S. C. Singh, J. W. Pye. Seismic evidence of a complex multi-lens melt reservoir beneath the 9° N Overlapping Spreading Center at the East Pacific Rise. Geophysical Research Letters, 2014, 41, pp.6109-6115. 10.1002/2014GL060859 . insu-03581102

HAL Id: insu-03581102
https://insu.hal.science/insu-03581102

Submitted on 19 Feb 2022

HAL is a multi-disciplinary open access archive for the deposit and dissemination of scientific research documents, whether they are published or not. The documents may come from teaching and research institutions in France or abroad, or from public or private research centers.

L'archive ouverte pluridisciplinaire **HAL**, est destinée au dépôt et à la diffusion de documents scientifiques de niveau recherche, publiés ou non, émanant des établissements d'enseignement et de recherche français ou étrangers, des laboratoires publics ou privés.

Copyright

AGU PUBLICATIONS

Geophysical Research Letters

RESEARCH LETTER
10.1002/2014GL060859

Key Points:
- We report a unique image of multiple stacked crustal melt lenses
- The complex reservoir is due to the reduced ambient stress regime from the overlap
- The multi-lens reservoir is the source of very evolved lavas

Correspondence to:
A. F. Arnulf,
aarnulf@ucsd.edu

Citation:
Arnulf, A. F., S. C. Singh, and J. W. Pye (2014), Seismic evidence of a complex multi-lens melt reservoir beneath the 9° N Overlapping Spreading Center at the East Pacific Rise, *Geophys. Res. Lett.*, *41*, 6109–6115, doi:10.1002/2014GL060859.

Received 11 JUN 2014
Accepted 7 AUG 2014
Accepted article online 11 AUG 2014
Published online 2 SEP 2014

Seismic evidence of a complex multi-lens melt reservoir beneath the 9° N Overlapping Spreading Center at the East Pacific Rise

A. F. Arnulf[1,2], S. C. Singh[1], and J. W. Pye[3]

[1]Équipe de Géosciences Marines, Institut de Physique du Globe de Paris (CNRS, Paris Diderot, Sorbonne Paris Cité), Paris, France, [2]Now at Cecil H. and Ida M. Green Institute of Geophysics and Planetary Physics, Scripps Institution of Oceanography, University of California San Diego, La Jolla, California, USA, [3]Premier Oil, Aberdeen, UK

Abstract The crustal structure at fast spreading ridges is characterized by the presence of an axial melt lens along a significant part of the ridge axis over a partially molten lower crust. Using three-dimensional seismic reflection data and waveform inversion, here we show the existence of two to three stacked melt lenses beneath both limbs of the 9°N overlapping spreading center on the East Pacific Rise, which we suggest are the source of the very evolved lavas locally observed on the seafloor. The melt lenses are 2–4 km wide and lie in a 900 m depth range. We suggest that the presence of a complex multi-lens melt reservoir in the crust is due to the reduced ambient stress regime, hence cracking, resulting from the overlap of the two segments of the ridge, allowing melt to stay longer in the crust at different depths.

1. Introduction

Seismic reflection studies from fast [*Detrick et al*., 1987], intermediate [*Collier and Sinha*, 1990] and slow spreading [*Singh et al*., 2006a] centers have shown the presence of upper crustal melt lenses (Axial Magma Chamber, AMC), which are believed to be at the top of partially molten lower crust [*Toomey et al*., 1990; *Vera et al*., 1990] where magma cools and crystallizes to form gabbroic lower crust [*Phipps Morgan and Chen*, 1993]. At fast spreading centers, these melt lenses are 250–4000 m wide [*Kent et al*., 1993] and often extend along the whole segment of the ridge. These observations have led to a model where the upper crust is formed by dike and pillow lavas whereas the lower crust by cooling and crystallization of magma in the thin melt lens [e.g., *Henstock et al*., 1993]. On the other hand, some petrological studies from Oman Ophiolite have suggested that the lower crust is formed by multiple-lens injections at different depths in the lower crust, below the main melt lens [*Kelemen et al*., 1997; *Boudier et al*., 1996].

So far, except from the anomalously magmatic Axial volcano that lies at the intersection of the Juan de Fuca ridge and the Cobb Eickerberg hot spot chain [*Arnulf et al*., 2014], only one reflection event associated with the axial melt lens has been imaged, which could be from the top of the melt lens or due to interference from the top and bottom of a thin melt lens. Using thin melt lens approximation and waveform modeling study, *Kent et al*. [1993] suggested that the melt lens should be 50–100 m thick. Using seismic full waveform inversion (FWI) method, *Singh et al*. [1998, 1999] found that melt lens at 14°S EPR is ~60 m thick and is underlain by a solid material because velocity just below the melt lens is the same as that above it. Similar melt lens thicknesses have been obtained for melt lenses at 9° 30′ EPR [*Collier and Singh*, 1997] and at the Cleft segment of the Juan de Fuca Ridge [*Canales et al*., 2006]. More recently, *Xu et al*. [2014] find melt lens to be 8–120 m thick at 9°42 and 9°50 N.

Singh et al. [1998] have shown that even though these melt lenses are thin and seem continuous on conventional seismic images, they are segmented into 2–4 km long pure melt and 15–20 km long mush regions, and proposed that the pure melt region corresponds to fresh supply of magma in the melt lens whereas mush zone is associated with cooled and crystallized part of the lens. A similar observation was reported for the Juan de Fuca ridge [*Canales et al*., 2006]. Additionally, *Carbotte et al*. [2013] have shown that these lenses are physically isolated, leading to the eruption of distinct lavas on the seafloor that coincide with the tectonic segmentation.

Here, we report a unique image of several stacked melt lenses at the 9°N overlapping spreading center (OSC), East Pacific Rise (EPR).

©2014. American Geophysical Union. All Rights Reserved.

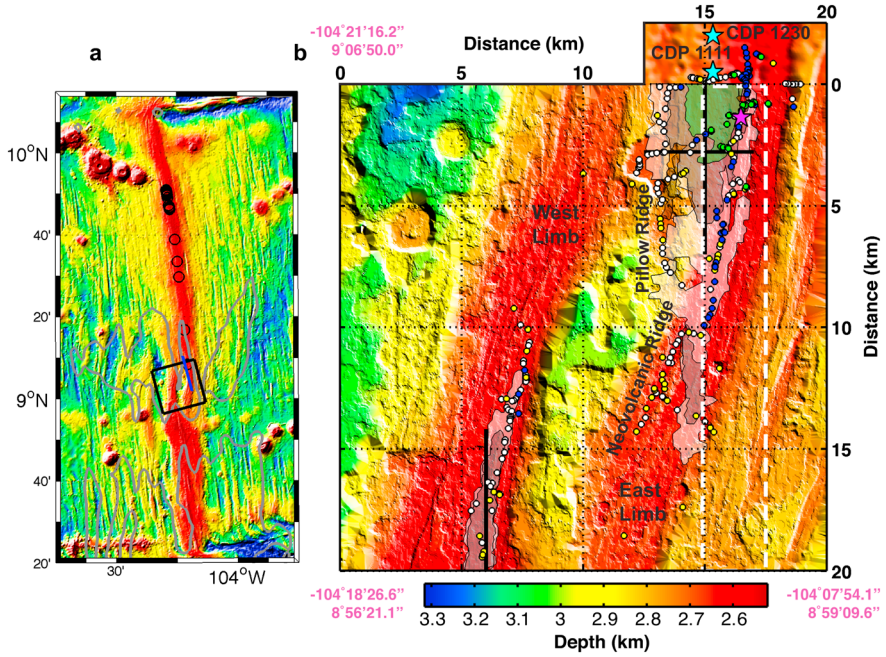


Figure 1. Three-dimensional (3D) seismic survey area and images of the stacked melt lenses. (a) Seafloor bathymetry of the 9°N segment of the East Pacific Rise (EPR) spreading center. The black square box indicates the location of the 3D seismic survey (Anatomy of a Ridge Axis Discontinuity (ARAD), shown in b), positioned over the overlapping spreading center (OSC). The 3D survey size is 20 × 20 km, and is oriented 15° anticlockwise from the north. The blue line shows the location of the Omega line, which is also oriented 15° anticlockwise from the north. Black circles indicate the hydrothermal vents. The grey line outlines region of high magnetization (>10, see: *Carbotte and Macdonald* [1992]). (b) Bathymetry of the seafloor derived from 3D seismic experiment. Locations of the stacked melt lenses are shown, from top to bottom, by green, white, and black areas. The dashed white box show the location of 3D seismic section shown, and the solid black lines show the location of 2D seismic sections (see Figure 2). Locations of lava samples collected during the MEDUSA cruise in 2007 are divided into rock types [*Wanless et al.*, 2010, 2012]: dacite (green circles), andesite and basaltic andesite (blue circles), FeTi basalt (yellow circles), and ferrobasalt (white circles). Purple hue star indicates location of the Medusa hydrothermal vent site [*Klein et al.*, 2013]. Cyan hue stars indicate locations of CMPs 1111 and 1230 used for a separate waveform inversion experiment (Figure 3, [*Pye*, 2002]).

2. Melt Lens and Magma Compositions at 9°N Overlapping Spreading Center (OSC)

The 9° OSC is a second-order discontinuity where the two limbs of the spreading center overlap for about 27 km and are offset by 8 km. The eastern limb of the OSC is propagating southward at a rate of 42 km/Ma, or about half of the present-day spreading-rate, whereas the western limb is receding [*Carbotte and Macdonald*, 1992]. Lavas from the OSC have an extensive range of compositions, including ferro-basalts, FeTi basalts as well as rarer high-silica andesites and dacites [*Wanless et al.*, 2010, 2012; *Waters et al.*, 2013], more evolved than typical mid-ocean ridge basalts (MORB), suggesting variable degrees of fractional crystallization, magma mixing, and crustal assimilation.

From a three-dimensional (3D) seismic reflection study, *Kent et al.* [2000] showed a very wide melt lens beneath the eastern limb of the OSC. Seismic tomographic studies image a low velocity anomaly in the lower crust [*Bazin et al.*, 2003] and upper mantle [*Dunn et al.*, 2001; *Toomey et al.*, 2007] underneath the melt lens, suggesting the presence of partial melt in the lower crust and upper mantle. The melt lens is at ~1650–2200 m depth beneath the seafloor, and its width varies from ~4.5 km in the north (Figure 1) to ~250 m in the south. On the eastern limb, the melt lens is asymmetric and lies mainly west of the ridge crest, while on the western limb, the melt lens lies beneath the ridge crest [*Combier et al.*, 2008].

Normally, it is difficult to image structures below the melt lens because of high attenuation of seismic energy traversing the melt lens. However, using 3D seismic reflection data *Singh et al.* [2006b] have imaged a reflection from the Moho discontinuity beneath the wide melt lens at the eastern limb of the OSC, but no secondary melt lens in the lower crust was reported.

©2014. American Geophysical Union. All Rights Reserved.

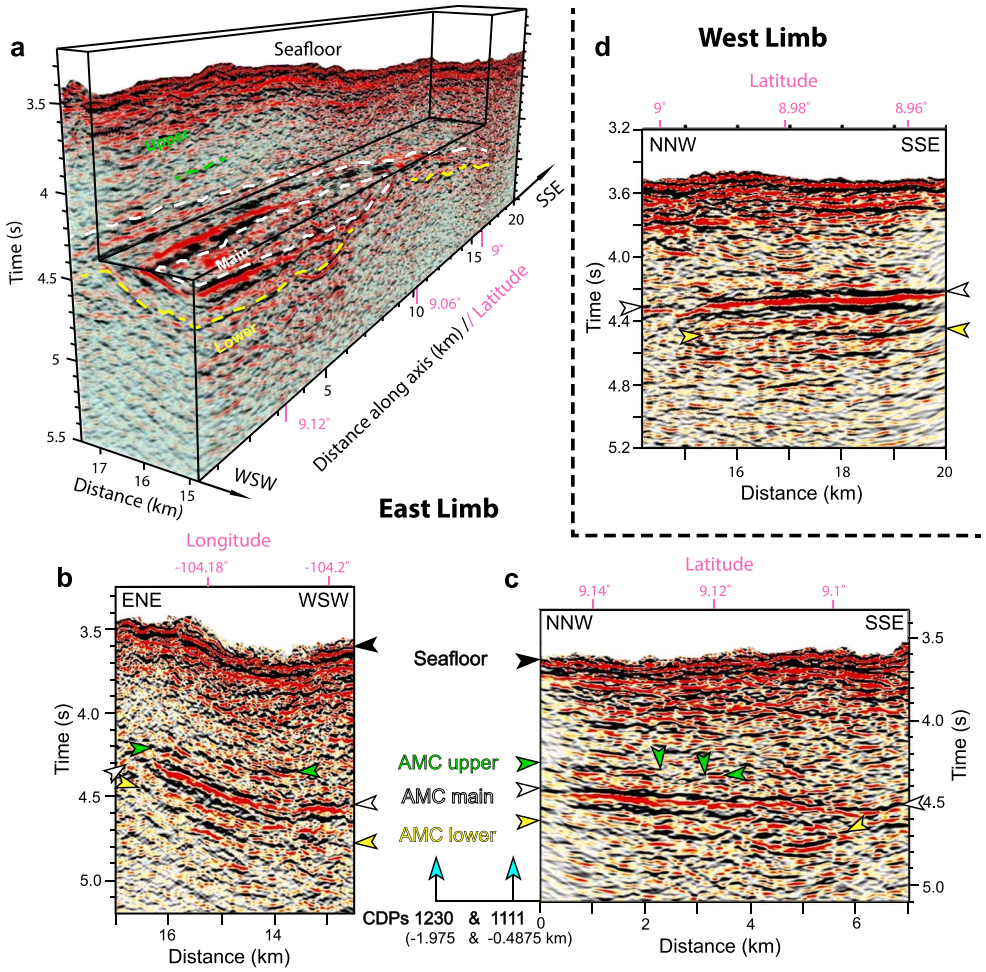


Figure 2. Extent of the stacked melt lenses. (a) A three-dimensional (3D) chair-cut view through the ARAD seismic reflectivity volume showing the main melt lens recognized by *Kent et al*. [2000] as well as lower and upper melt lenses. The view is from northwest looking at along axis towards south (ahead) and across axis towards east (left). (b) Across axis seismic section at 2800 m within the 3D box; (c) along axis section at 14,950 m; and (d) along axis section at 6000 m that allows to get some sense of 3D extent of the stacked melt lenses. Cyan arrows indicate locations of CDPs 1111 and 1230 used for a separate waveform inversion experiment (Figure 3, [*Pye*, 2002]).

3. Data and Methods

The 1997 ARAD (Anatomy of a Ridge Axis Discontinuity) 3D seismic reflection data [*Kent et al*., 2000; *Singh et al*., 2006b] were acquired within a $20 \times 20\ km^2$ box onboard the R/V *Maurice Ewing* using a 3100 m long streamer. The data consisted of a series of 201 cross-axis profiles separated by 100 m, with 25 m receiver group spacing and in-line shot spacing of 37.5 m. Processing included dip-moveout correction along the 2D profiles, 3D common-midpoint (CMP) binning onto a 12.5×100 m grid, velocity analysis, stacking of source-receiver offsets up to 2300 m offset down to the melt lens and up to 3100 m down to the Moho. Finally, inline Kirchhoff migration was applied followed by 3D interpolation onto a 25×25 m grid and cross-line Kirchhoff migration.

To better characterize the nature of the geometrically complex melt reservoir, one-dimensional (1D), full waveform inversion (FWI) was also conducted to the northwest of the 3D box [*Pye*, 2002]. Details about the inversion procedure used in this study can be found elsewhere [*Collier and Singh*, 1997]. Two locations along the ridge parallel Omega line, CMP 1111 and CMP 1230 (Figure 1), were selected because of the locally flat seafloor and AMC reflector for which the 1D approximation is valid. The inversion provided the detailed velocity structure near the AMC by minimizing the misfit between observed and synthetically calculated data.

©2014. American Geophysical Union. All Rights Reserved.

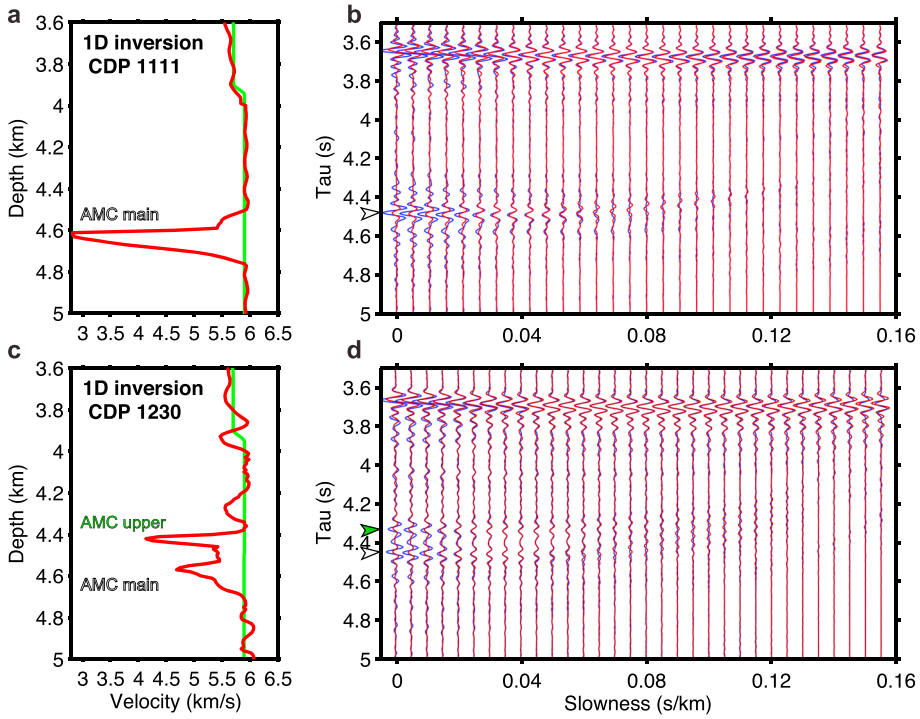


Figure 3. Axial melt reservoir waveform inversion results. Starting (green line, [*Vera et al.*, 1990]) and final velocity structure (red line) at CMP 1111 (a) and CMP 1230 (c). Final synthetic seismograms in red plotted with the same gain as the observed data in blue at CMP 1111 (b) and CMP 1230 (d). Both CMP gathers are transformed in the τ-p domain. CMP 1111 shows a strong seafloor reflection (~3.65 s) as well as a *P*-wave reflection from the main melt lens at near vertical incident angles (white arrow at ~4.5 s). CMP 1230 shows a strong seafloor reflection (~3.65 s) followed by two distinct *P*-wave reflections from the main and upper melt lenses at near vertical incident angles (white and green arrows at ~4.5 and ~4.3 s, respectively).

4. Stacked Melt Lenses at 9°N Overlapping Spreading Center (OSC)

Beneath both limbs of the OSC, the 3D seismic reflection data show the presence of a second reflection 150–250 ms below the interpreted main melt lens reflector reported by *Kent et al.* [2000] (AMC main and lower reflectors on Figure 2). Polarity of this reflection is complex due to the interference effect. Since the dominant frequency of the data is 10–25 Hz, this arrival could be due to the bubble pulse or ringing effect, but no such arrivals are associated with the seafloor reflection in the 3D volume. Furthermore, the bubble pulse with 10 Hz would be 100 ms below the main arrival whereas this reflection is 150–250 ms beneath the main melt lens reflection. A multiple reflection or PmeltS reflection will follow the main melt lens reflection, but this reflection locally pinches out and does not follow the top of the main melt lens reflection (Figure 2). This reflection could either be a secondary melt lens in the lower crust or the bottom of the main melt lens. Since the lower reflection is rather weak it is difficult to determine the precise lateral extent (Figure 2b), but one can clearly observe it at the northern end of the eastern limb, continuing up to ~5.5 km southwards (Figures 2a and 2c). It is about 3 km wide in the north and then narrows down in the south (Figure 1). Beneath the western limb, its width is similar to the main melt lens and it extends ~5.5 km northwards following the ridge crest. This secondary deeper reflection seems to be present beneath the melt-rich regions determined from amplitude versus offset [*Singh et al.*, 2006b] and to a greater extent above the large lower crustal melt anomaly [*Bazin et al.*, 2003]. Interestingly, a third shallow crustal reflector (namely: AMC upper, see: Figure 2), is also observed 100–200 ms above the main melt lens reflector at the northern end of the 3D box. The lower reflectivity of this shallow reflector compared to the underlying bright reflection of the main melt lens likely suggests the presence of a melt-depleted lens overlying the main reservoir.

The results of full waveform inversion are shown in Figure 3. Although the locations of the waveform inversion sites are outside of the 3D box, these results provide insight about the nature of the melt lenses. By looking at the data, the stacked melt lens reflections can be traced at near vertical incident angle (see Figure 3d), testifying that crustal changes in acoustic impedance are strong enough to create several *P* wave reflections. The fit

©2014. American Geophysical Union. All Rights Reserved.

between the predicted seismograms and observed data is 85% and 90% for CMPs 1111 and 1230, which gives confidence in the inversion results (Figures 3b and 3d). While the average mid-crustal background velocity (~6 km/s) is similar at both CMP locations, the melt reservoir is geometrically and physically different. The final velocity model for CMP 1111 displays a single, thin, supposedly melt-rich, lens-like structure with minimum *P* wave velocity of 2.8 km/s, underlain by a slightly thicker interval of increasing velocity, which could be interpreted as a zone of partial melt. On the other hand, at CMP 1230, two independent melt-depleted lenses are observed. The *P* wave velocity structure drops to 4.1 km/s within the upper lens then levels up to 5.35 km/s within a ~80 m region before dropping to 4.6 km/s within the upper part of the deeper lens to finally gradually increasing to reach the typical mid-crustal velocity background, suggesting the presence of two independent melt lenses. Due to the proximity of the waveform inversion study sites with the 3D migrated box, we suggest that the reflectors observed on the reflection data (Figure 2) correspond to a series of stacked melt lenses.

5. Discussion

Singh et al. [2006b] observed a large travel time (600 ms) anomaly between the Moho and the melt lens in this region. They attributed a part of this lower crustal anomaly to a thicker crust and a part of it to a large melt throughout lower crust. The ~450 ms thick region of stacked melt lenses (Figure 2) could account for ~25–32% of the lower crustal travel time anomaly assuming *P* wave velocities of 3.5–4 km/s. Therefore, most of the anomaly could be explained by the presence of melt in a series of melt lenses and in the lower crust beneath it, and the thickening of the crust would not be required.

If we assume a *P* wave velocity of 3.5–4 km/s in the region where we observed the three stacked lenses (~450 ms), the melt reservoir would be up to 750–900 m. If we take an average thickness of 400 m over $5.5 \times 2.5\ km^2$ (the area of stacked melt lenses), and we use a differential effective medium theory [*Taylor and Singh*, 2002] to estimate melt fraction from the seismic velocity structure (55–80%), the total volume of pure melt beneath the eastern limb would be 3–4.4 km^3, not including the melt in the thin portion of the melt lens and the melt in the lower crust. Similarly, beneath the western limb, the total volume of pure melt would be 0.6–0.9 km^3.

There are several explanations for the presence of a complex, wide (4.5 km) and multi-lens melt reservoir. First, the supply of melt from the mantle could be west of the recent eruptive centers, and since the melt has to channel to these eruptive centers, it could form a series of wide melt lenses [*Kent et al*., 2000; *Combier et al*., 2008]. However, since the melt lenses have a dip (Figure 2b), the melt would flow upwards and would erupt in the presence of cracks. Second, the supply of the melt from the mantle could be excessively large; in which case the crust would be excessively thick. There is some indication of thick crust [*Canales et al*., 2003], but it is not excessively thick. The third possibility is that melt does not get squeezed out by eruption but resides in the crust much longer time than its counterpart further north, where only a single narrow lens has been imaged [*Xu et al*., 2014], though recent conflicting results also suggest a series of stacked lenses in that area [*Marjanovic*, 2013]. This could be due to the reduced ambient stress regime [*Combier et al*., 2008; *White et al*., 2009], and hence cracking [*Klein et al*., 2013], because of the overlap where the spreading rate at the western side of the limb is reduced by a factor of two. This would have an effect on the type of lava erupted. Long residence times of a mafic melt within a series of stacked lenses (Figure 2) would favor fractional crystallization, a necessary process to produce the evolved ferro-basalts and FeTi basalts sampled on both limbs [*Wanless et al*., 2010, 2012]. Furthermore, the presence of a series of shallow thin melt lenses at the northern end of the 3D box (Figure 2), adjacent to an active vent site (Figure 1), could explain the presence of silica rich andesites and dacites flows in this area. In fact, previous geochemical observations [*Wanless et al*., 2010, 2012; *Waters et al*., 2013] suggest that the formation of the high-silica tholeiitic rocks from the eastern limb of the OSC is likely the results of high level of fractional crystallization (~60%), magma mixing, crustal assimilation, and contamination from a seawater-altered component in a series of shallow thin melt lenses or in a thin viscous dacitic "cupola" on top of the main reservoir. Phenocryst abundances in 9°N OSC lavas also suggest that basalts from the pillow ridge and the neovolcanic ridge tap a deeper magma reservoir compared to the silica-rich axial magmas [*Klein et al*., 2013], which is in good agreement with our geophysical observations of stacked lenses. In such a model, melt delivery at the neovolcanic and pillow ridges would occur through laterally propagating dikes taping one of the deeper melt lenses. A previous tomographic study also suggests that layer 2A is thin above the stacked melt lenses (~0.4 km) and only slightly thickens

©2014. American Geophysical Union. All Rights Reserved.

westward [*Tong et al*., 2003]. However, it is not very thick as required for an excessively large melt supply model. Therefore, we suggest that one of the main reasons for the presence of wide and complex stacked melt lenses beneath the OSC is the poor melt extraction process. This process could also explain the presence of a wide melt lens beneath the OSC at the Valu Fa Ridge [*Collier and Sinha*, 1990].

Is there an inverse relationship between the width and vertical complexity (stacked lenses) of the melt reservoir and volcanic eruption effusion rate at the EPR? Seismic study shows thin melt lens near 9°50′ N [*Xu et al*., 2014] where the eruption is more frequent [*White et al*., 2009], whereas it is less frequent near 9°N where a very wide and complex melt reservoir is observed. The eruption rate depends on melt supply, pressure in the melt lens, density and viscosity of melt, and ambient stress field responsible for cracking. Since the presence of the OSC decreases the ambient ridge normal stress field and hence cracking, the effect of which would be maximum near the OSC and will decrease northward. If this is the case, the width and vertical complexity of the melt lens could reflect the ambient stress regime, and could be used as an indication for the stress field variations along the ridge axis. *White et al*. [2002] have also observed a correlation between along axis variations in melt lens, geochemistry of basalts, lava morphology (from sheet to pillow flows), and volcanic activity. It is possible that the morphological and volcanic segmentations observed along the 9°N of EPR might be linked to this change in stress field.

6. Conclusions

We imaged a series of stacked melt lenses beneath the eastern limb of the OSC, which outline a complex melt reservoir up to ~900 m thick. We suggest that the presence of a series of stacked melt lenses in the crust is due to reduced ridge-normal stress because of the overlap leading to slow cracking and hence less eruption allowing melt to stay longer in the crust. We suggest that the shallowest thin melt lens, at the northeastern side of the OSC, could be the source of the very evolved lavas observed locally. The long residence time of the magma in these melt lenses would lead to significant degrees of fractional crystallization, crustal assimilation, and possible magma mixing between the two-three stacked lenses, and would erupt an extensive range of evolved lavas, which is confirmed by the geochemical observations of erupted lavas [*Wanless et al*., 2010, 2012; *Waters et al*., 2013].

Acknowledgments

The 3D seismic reflection data were acquired onboard RV *Maurice Ewing*, processed by Robertson Research Ltd, and interpreted using the 3D VoxelGeo software of Paradigm Geophysical. The ARAD seismic experiment was an international collaborative project between investigators from the University of Cambridge and Scripps Institution of Oceanography and was funded by the UK Natural Environment Research Council, the British Institutions Reflection Profiling Syndicate, and the United States National Science Foundation. This research was carried out at the Institut de Physique du Globe de Paris as well as at the Scripps Institution of Oceanography. The "Ministère Français de l'enseignement supérieur et de la recherche" supported this work. This research was additionally supported through the Cecil H. and Ida M. Green Foundation at the Scripps Institution of Oceanography. This study also benefited from reviews by two anonymous reviewers. The data for this paper are available at http://www.marine-geo.org/tools/new_search/index.php?&a=1&funding=Ridge2000&output_info_all=on&entry_id=EW9707.

The Editor thanks Scott White and an anonymous reviewer for their assistance in evaluating this paper.

References

Arnulf, A. F., A. J. Harding, G. M. Kent, S. M. Carbotte, J. P. Canales, and M. R. Nedimovic (2014), Anatomy of an active submarine volcano, *Geology*, *48*(8), 655–658, doi:10.1130/G35629.1.

Bazin, S., et al. (2003), A three-dimensional study of axial low velocity region beneath the 9°03′ overlapping spreading centre, *Geophys. Res. Lett.*, *30*, 1039, doi:10.1029/2002GL015137.

Boudier, F., A. Nicolas, and B. Ildefonse (1996), Magma chambers in the Oman ophiolite, fed from the top and the bottom, *Earth Planet. Sci. Lett.*, *144*, 239–250.

Canales, J. P., R. S. Detrick, D. R. Toomey, and W. S. D. Wilcock (2003), Segment-scale variations in the crustal structure of 150-300 kyr old fast spreading oceanic crust (East Pacific Rise, 8° 15′ N–10° 5′ N) from wide-angle seismic refraction profiles, *Geophys. J. Int.*, *152*, 766–794.

Canales, J. P., S. C. Singh, R. S. Detrick, S. M. Carbotte, A. J. Harding, G. M. Kent, J. B. Diebold, J. Babcock, and M. R. Nedimovic (2006), Seismic evidence for variations in axial magma chamber properties along the southern Juan de Fuca Ridge, *Earth Planet. Sci. Lett.*, *246*, 353–366.

Carbotte, S., and K. C. Macdonald (1992), East Pacific Rise 8°–10°30′N: Evolution of ridge segments and discontinuities from SeaMARC II and three-dimensional magnetic studies, *J. Geophys. Res.*, *97*, 6959–6982, doi:10.1029/91JB03065.

Carbotte, S. M., M. Marjanovic, H. Carton, J. C. Mutter, J. P. Canales, M. R. Nedimovic, S. Han, and M. R. Perfit (2013), Fine-scale segmentation of the crustal magma reservoir beneath the East Pacific Rise, *Nat. Geosci.*, *6*, 866–870, doi:10.1038/NGEO1933.

Collier, J. S., and S. C. Singh (1997), Detailed structure of the top of the melt body beneath the East Pacific Rise at 9°40 N from waveform inversion of seismic reflection data, *J. Geophys. Res.*, *102*, 20,287–20,304, doi:10.1029/97JB01514.

Collier, J., and M. C. Sinha (1990), Seismic images of a magma chamber beneath the Lau Basin back-arc spreading centre, *Nature*, *346*, 646–648.

Combier, V., S. C. Singh, M. Cannat, and J. Escartin (2008), Mechanical decoupling and thermal structure at the East Pacific Rise axis 9°N: Constraints from axial magma chamber geometry and seafloor structures, *Earth Planet. Sci. Lett.*, *272*, 19–28.

Detrick, R. S., P. Buhl, E. Vera, J. Mutter, J. Orcutt, J. Madsen, and T. Brocher (1987), Multi-channel seismic imaging of a crustal magma chamber along the East Pacific Rise, *Nature*, *326*, 35–41.

Dunn, R. A., D. R. Toomey, R. S. Detrick, and W. S. D. Wilcock (2001), Continuous mantle melt supply beneath an overlapping spreading centre on the East Pacific Rise, *Science*, *291*, 1955–1958.

Henstock, T. J., A. W. Woods, and R. S. White (1993), The accretion of oceanic crust by episodic sill intrusion, *J. Geophys. Res.*, *98*, 4143–4161, doi:10.1029/92JB02661.

Kelemen, P. B., K. Koga, and N. Shimizu (1997), Geochemistry of gabbro sills in the crust-mantle transition zone of the Oman ophiolite: Implications for the origin of the oceanic lower crust, *Earth Planet. Sci. Lett.*, *146*, 475–488.

Kent, G. M., A. J. Harding, and J. A. Orcutt (1993), Distribution of magma beneath the East Pacific Rise between the Clipperton Transform and the 9° 17′ N Deval from forward modelling of common depth point data, *J. Geophys. Res.*, *98*, 13,945–13,969, doi:10.1029/93JB00705.

©2014. American Geophysical Union. All Rights Reserved.

Kent, G. M., et al. (2000), Evidence from three-dimensional reflectivity images for enhanced melt supply beneath mid-ocean-ridge discontinuities, *Nature*, *406*, 614–618.

Klein, E. M., et al. (2013), Seafloor photo-geology and sonar terrain modeling at the 9°N overlapping spreading center, East Pacific Rise, *Geochem. Geophys. Geosyst.*, *14*, 5146–5170, doi:10.1002/2013GC004858.

Marjanovic, M. (2013), Signatures of present and past melt distribution at fast and intermediate spreading centers, PhD thesis, Columbia Univ., New York.

Phipps Morgan, J., and Y. Chen (1993), Genesis of oceanic crust: Magma injection, hydrothermal circulation, and crustal flow, *J. Geophys. Res.*, *98*, 6283–6298, doi:10.1029/92JB02650.

Pye, J. W. (2002), Three-dimensional crustal structure of the East Pacific Rise at 9°N, PhD thesis, Univ. of Cambridge, Cambridge, U. K.

Singh, S. C., G. M. Kent, J. S. Collier, A. J. Harding, and J. A. Orcutt (1998), Melt to mush variations in crustal magma properties along the ridge crest at the southern East Pacific Rise, *Nature*, *394*, 874–878.

Singh, S. C., J. S. Collier, G. M. Kent, A. J. Harding, and J. A. Orcutt (1999), Seismic evidence for a hydrothermal layer above the solid roof of axial magma chamber at the southern East Pacific Rise, *Geology*, *27*, 219–222.

Singh, S. C., W. Crawford, H. Carton, T. Seher, V. Combier, M. Cannat, J. P. Canales, D. Dusunur, J. Escartin, and M. Miranda (2006a), Discovery of a magma chamber and faults beneath a hydrothermal field at the Mid-Atlantic Ridge, *Nature*, *442*, 1029–1033.

Singh, S. C., et al. (2006b), Seismic reflection images of Moho underlying melt sills at the East Pacific Rise, *Nature*, *442*, 287–290.

Taylor, M. A. J., and S. C. Singh (2002), Composition and microstructure of magma bodies from effective medium theory, *Geophys. J. Int.*, *149*, 15–21.

Tong, C. H., et al. (2003), Influence of enhanced melt supply on upper crustal structure at a mid-ocean ridge discontinuity: A three-dimensional seismic tomographic study of 9°N East Pacific Rise, *J. Geophys. Res.*, *108*, 2464, doi:10.1029/2002JB002163.

Toomey, D. R., G. M. Purdy, S. C. Solomon, and W. S. D. Wilcock (1990), The three-dimensional seismic velocity structure of the East Pacific Rise near latitude 9°30′ N, *Nature*, *347*, 639–645.

Toomey, D. R., D. Jousselin, R. A. Dunn, W. Wilcock, and R. S. Detrick (2007), Skew of mantle upwelling beneath the East Pacific Rise governs segmentation, *Nature*, *446*, 409–414.

Vera, E. E., J. C. Mutter, P. Buhl, J. A. Orcutt, A. J. Harding, M. E. Kappus, R. S. Detrick, and T. M. Brocher (1990), The structure of 0 to 0.2 m.y. old oceanic crust at 9° N on the East Pacific Rise from expanding spread profiles, *J. Geophys. Res.*, *95*, 15,529–15,556, doi:10.1029/JB095iB10p15529.

Wanless, V. D., M. R. Perfit, W. I. Ridley, and E. M. Klein (2010), Dacite petrogenesis on mid-ocean ridges: Evidence for oceanic crustal melting and assimilation, *J. Petrol.*, *51*(12), 2377–2410.

Wanless, V. D., M. R. Perfit, E. M. Klein, S. White, and W. I. Ridley (2012), Reconciling geochemical and geophysical observations of magma supply and melt distribution at the 9°N overlapping spreading center, East Pacific Rise, *Geochem. Geophys. Geosyst.*, *13*, Q11005, doi:10.1029/2012GC004168.

Waters, C. L., K. W. W. Sims, E. M. Klein, S. M. White, M. K. Reagan, and G. Girard (2013), Sill to surface: Linking young off-axis volcanism with subsurface melt at the overlapping spreading center at 9°03′N East Pacific Rise, *Earth Planet. Sci. Lett.*, *369*, 59–70.

White, S. M., R. M. Haymon, D. J. Fornari, M. R. Perfit, and K. C. Macdonald (2002), Correlation between volcanic and tectonic segmentation of fast-spreading ridges: Evidence from volcanic structures and lava flow morphology on the East Pacific Rise at 9°–10° N, *J. Geophys. Res.*, *107*, 2173, doi:10.1029/2001JB000571.

White, S. M., J. L. Mason, K. C. Macdonald, M. R. Perfit, V. D. Wanless, and E. M. Klein (2009), Significance of widespread low effusion rate eruptions over the past two million years for delivery of magma to the overlapping spreading centers at 9°N East Pacific Rise, *Earth Planet. Sci. Lett.*, *280*, 175–184, doi:10.1016/j.epsl.2009.01.030.

Xu, M., J. P. Canales, S. M. Carbotte, H. Carton, M. R. Nedimovic, and J. C. Mutter (2014), Variations in axial magma lens properties along the East Pacific Rise (9°30′N-10°00′N) from swath 3-D seismic imaging and 1-D waveform inversion, *J. Geophys. Res. Solid Earth*, *119*, 2721–2744, doi:10.1002/2013JB010730.

©2014. American Geophysical Union. All Rights Reserved.